The Effect of Modulation Frequency for Frequency Domain Diffuse Optic Tomography (FDDOT)

Huseyin Ozgur Kazanci (ozgurkazanci@gmail.com)
Akdeniz University Faculty of Engineering https://orcid.org/0000-0003-0036-7657

Research Article

Keywords: Diffuse Optic Tomography (DOT), Frequency Domain Diffuse Optic Tomography (FDDOT), Modulation Frequency, Phase Delay.

Posted Date: March 31st, 2021

DOI: https://doi.org/10.21203/rs.3.rs-376074/v1

Version of Record: A version of this preprint was published at Optical and Quantum Electronics on March 1st, 2022. See the published version at https://doi.org/10.1007/s11082-022-03595-x.

The Effect of Modulation Frequency for Frequency Domain Diffuse Optic Tomography (FDDOT)

Huseyin Ozgur Kazanci [1,*]

[1] *Akdeniz University, Faculty of Engineering, Department of Biomedical Engineering, Antalya, Turkey, 07058 +90-242-3106300 ext.4302*

* *Corresponding author: ozgurkazanci@akdeniz.edu.tr*

Abstract. In this study, it was illustrated that extremely high frequency (EHF) Ka-band (26.5-40 GHz) modulated frequency domain diffuse optic tomography (FDDOT) biomedical optic imaging (BOI) modality is superior to the generally accepted 100 MHz modulation frequency case. The effect of modulation frequency was shown with reconstructed images for two different modulation frequency simulation cases. Ka EHF-band frequency range covers 26.5 - 40 GHz. In this simulation study 33 GHz modulation frequency was selected. Forward model problem photon fluencies were generated for 30 equally separated sequential phase delays. Each phase delay has different photon fluence distributions inside the imaging geometry. 3.1 cm grid sizes were set in the x, y, z cartesian grid coordinate system with 31×31×31 xyz grid elements. To test the advantage of EHF-band modulation frequecy, inverse problem solution algorithm was done and inclusion images were reconstructed for each modulation frequency simulation case. Original inclusion was embedded inside the imaging geometry at (15-16, 15-16, 15-16) x, y, z coordinate system in the three-dimensional (3D) cubic spatial form. Homogeneuous tissue background photon absorption, scattering, and anisotropy coefficients were selected as $\mu_a = 0.1$ cm^{-1}, $\mu_s = 100$ cm^{-1}, and $g = 0.9$. Four sources and four detectors were placed on the back-reflection geometry. Forward model problem was built between sources, voxels, and detectors. Forward model problem photon fluencies were generated based on the diffusion equation (DE) approximation of the radiative

transport equation (RTE) formula in the frequency domain. Original inclusion was reconstructed by simply applying mathematical pseudoinverse problem solution function. It was observed that, reconstructed inclusion image at the 33 GHz Ka-Band modulation frequency simulation case is superior to the reconstructed inclusion image at the 100 MHz modulation frequency simualtion case. Since there are too many frequency selection opportunities, the best Ka-band frequency was selected to demonstrate here. Thus, 33 GHz and 100 MHz modulation frequencies were tested against each other. These two different electronic modulation frequencies were tested and compared with each other.

Keywords: Diffuse Optic Tomography (DOT), Frequency Domain Diffuse Optic Tomography (FDDOT), Modulation Frequency, Phase Delay.

OCIS codes: 100.3010 Image Reconstruction Techniques, 100.3190 Inverse Problems, 140.3518 Lasers, Frequency Modulation, 170.3660 Light Propagation in Tissues, 110.6955 Tomographic Imaging.

I. INTRODUCTION

Diffuse Optic Tomography (DOT) systems run based on the three different modes which are basically known as continuous wave (CW), time resolved (TR), and frequency domain (FD). Frequency domain (FD) diffuse optical tomography (FDDOT) modality is one of the biomedical optical mammography, neuronal brain activity, and blood oxygen saturation imaging methods. DOT modality uses forward model problem photon transport equation depend on the homogeneous background tissue type. Photon migration inside the tissue is modelled by diffusion approximation of radiative transport equation (RTE) or photon particle model which uses Monte

Carlo (MC) photon-tissue interaction simulations. DOT imaging modality has been tested, reviewed, and discussed [1-5]. General terms of DOT imaging modality and its application fields in clinic has been given [1]. FDDOT imaging modality was also mentioned, and application fields have been given [1]. 50-100 MHz modulation frequency range was used for different time and spatial dependent situations [2]. Source-detector placement on the imaging surface is very important step for noise reduction and improving image quality for especially calculation of hemoglobin concentration and evaluation of physiological response to brain activation. Source - detector neighborhood relations were analyzed, and better placement schema was configured with the help of MRI data [3]. In this work, the source and detector nodes were placed on the back-reflection geometry based on the help of neighborhood relation which were mentioned earlier [3]. Since the main motivation of near infrared DOT imaging modality is differentiation of oxy- and deoxy-hemoglobin of blood content whether it works for breast tumor or brain blood neuro physiological activation, another possible investigation scenario is testing the oxygenation level of muscles related to the respiration which was studied [4]. Two different wavelengths 690 nm and 830 nm laser sources with the Continuous Wave (CW) mode were used [5]. Finger tapping exercise was tested to investigate the blood volume concentration differences. These works [1-5] are giving general concepts of DOI modality by using different methods for different clinic application fields which are essential to be able to correctly evaluate imaging method' s advantages and disadvantageous. Mostly, DOT imaging systems are used for the breast tumours (positive oxy and deoxy-hemoglobin perturbations) and neuronal brain (negative oxy and deoxy-hemoglobin perturbations) imaging purposes. In this work, diffusion approximation of RTE model was chosen at frequency domain. Modulation frequency is the key factor for FDDOT biomedical optic imaging (BOI) modality. Most of the researchers have been doing their FDDOT experiments at the 100

MHz center core modulation frequency. The effect of modulation frequency for FDDOT was studied in this work. FDDOT system design and manufacturing procedures were demonstrated for breast cancer detection [6-15]. One of the important efforts has been accomplished for frequency-domain breast-cancer detection system [6]. 32 laser diodes and photo-multiplier unit (PMT) was used. 100 MHz modulation frequency was selected in that work [6]. Three different wavelengths 684 nm, 794 nm, and 850 nm for three different chromophores which are oxygenated hemoglobin, deoxygenated hemoglobin and fat were used for FDDOT imaging system [7]. In that work, instead of using 100 MHz modulation frequency, 140 MHz modulation frequency was used [7]. To show the different variety of modulation frequency which was generally used and tested at the 100 MHz frequency, this work was given as a special example [7]. Some researchers have increased their source-detector matches and grouped their experimental measurements for especially head brain imaging at the frequency domain [8]. Neighborhoods grouping and selection of the best group approach was used in our work. In FDDOT imaging systems, only amplitude, only phase or both amplitude and phase components can be used differently. In the spatial frequency domain, forward model photon fluence weight matrix coefficients were calculated by using Monte-Carlo (MC) simulation method [9]. Since our study was mostly focused on the selection of modulation frequency, core modulation frequencies were searched based on the literature works. One of these works used different frequencies between 5 MHz and 250 MHz [10]. They searched for multiple modulation frequencies to investigate the optical properties. Some researchers have tried to combine different run modes such as, CW and FD run modes. They both used and tested to find the tissue absorption and scattering coefficients in spatial form [11]. They used the FD data to calibrate the CW laser source which involves many frequency components. They tried to find the total hemoglobin concentration, and oxygen saturation for the breast tissue. Since this work gives

an important idea to place the sources and detectors on the back-reflection imaging geometry for frequency-domain, it was used in our work to determine the source and detector placements. We defined the special source-detector configuration on the back-reflection geometry. We extracted useful neighborhood distance groups from this knowledge for image reconstruction. In most of the literature works, 100 MHz modulation frequency was used but on the contrary, in one study 500 MHz modulation frequency was used [12]. The example of well-established reference design for 100 MHz modulation signal instruments was also demonstrated 2 decades ago [13]. In one work it was shown that different modulation frequencies sweep technique can also be used to find the most proper frequency to calculate the tissue blood absorption coefficients in spatially performed region of interest (ROI) by using 780 nm laser wavelength [14]. They swept the modulation frequency between 30 and 700 MHz. 67.5 and 75 MHz modulation frequencies were also used and tested with high-speed analog to digital conversion (ADC) rate [15]. Finally, it was summarized that frequencies were selected between 30 MHz and 1 GHz. But the frequency modulation effect has never been evaluated until now which is very important for better instrumentation, data acquisition and image reconstruction phases. Important works have been gathered here, to give examples of modulation frequencies. Frequency domain diffusion equation (DE) formula was given [16]. Modulation frequency dependency was studied around 100 MHz and its multiple times [17]. In this work, instead of using 100 MHz, extremely high frequency (EHF) Ka-Band 33 GHz modulation frequency was used. For this purpose, FD DE was used at both frequencies. Photon transport fluencies at 33 GHz modulation frequency with 30 different phase shifts which were consecutively increased by 20 Hz were generated and translated through image reconstruction algorithm program environment. Inclusion molecule was embedded inside the imaging geometry then it was reconstructed by using pseudoinverse problem solution method.

II. METHODS

Ka EHF-band electronic core modulation frequency with 30 different phases were consecutively increased by 20 Hz. Frequency domain diffusion approximation for RTE was used [16]. Back-reflected imaging geometry was chosen to test the two different modulation frequencies. Four sources and four detectors were placed on top of the imaging tissue simulation background as seen in Figure 1. Sources are red circles, and detectors are blue squares. 3.1 cm × 3.1 cm × 3.1 cm x, y, z cartesian grid coordinate system with 31 grid elements for each axis were used. Photon fluence distributions were calculated for each source-detector (SD) match according to the diffusion equation (DE) in the frequency domain [16]. In Equation 1, forward model weight matrix was illustrated as *W*. Photon fluencies are from each source position to each voxel position (*SV*), and from each voxel position to each detector position (*VD*).

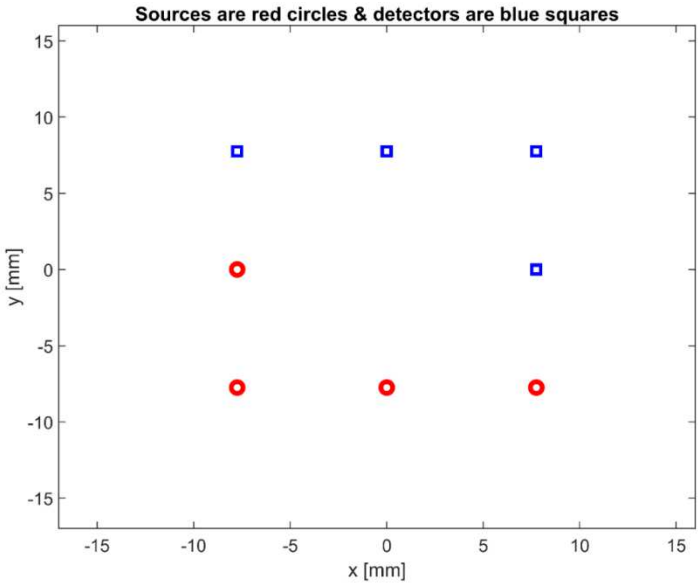

Figure 1. Four laser sources (red circles) and four detectors (blue squares) top view placement.

$$W = \frac{e^{j\times k\times d_{SV}}}{4\pi\times c\times D\times d_{SV}} \times \frac{e^{j\times k\times d_{VD}}}{4\pi\times c\times D\times d_{VD}} \qquad Equation\ 1.$$

$$k = \sqrt{\frac{-c \times \mu_a + j(2\pi f + \Delta\varphi)}{c \times D}}$$

$$D = \frac{1}{3\times(\mu_a+\mu_s')}$$

From each source position to each voxel position distance was illustrated as d_{SV} and each voxel position to each detector position distance was illustrated as d_{VD}. Modulation index k is the product of c light speed in the tissue, homogeneous background each voxel' s photon absorption coefficient μ_a, each voxel' s reduced photon scattering coefficient μ_s', imaginer constant j, phase degree π, modulation frequency f, and added phase delay $\Delta\phi$. D is the diffusion coefficient for specific homogeneous tissue type. 30 sequential phase photon fluencies were generated at 100 MHz, and 33 GHz EHF Ka-band frequencies, which were consecutively increased by 20 Hz. Homogeneous tissue background absorption coefficient μ_a = 0.1 cm^{-1}, and scattering coefficient μ_s = 100 cm^{-1}. Forward model problem was set based on the Equation 2. This is the linearized form of the diffusion equation which transforms important relation between photon fluencies and measurement or simulation data. In our case, we used simulation data. Equation 2 is representing forward model problem matrix calculation. W is the forward model problem weight matrix which involves weight coefficients for each voxel calculated from Equation 1. Our homogeneous background simulation model has W forward model matrix which of each voxel coefficients were calculated from Equation 1. X is the unknown absorption coefficient perturbation differences over homogeneous simulation background. Y is the simulation output data which was pre-given to the inverse problem solution algorithm described by the Equation 3.

$$W \times x = y \qquad Equation\ 2.$$

$$x = W^{\dagger} \times y \qquad Equation\ 3.$$

First, *W* weight matrix coefficients were calculated, and *W* matrix was built. In the second phase, *W* weight matrix and *x* homogeneous background absorption coefficients, with the addition of specific voxels heterogeneous inclusion were multiplied in matrix form, as a result *y* simulation data were obtained. In the final process, pseudo-inverse of the *W* weight matrix and *y* data vector were matrix multiplied based on the Equation 3 which was derived from Equation 2 by simply making pseudo-inverse multiplication of both sides, and unknowns were obtained. After calculating the *x* unknowns, *x* unknowns were placed in the three-dimensional (3D) image reconstruction volume, which shows reconstructed inclusion image.

III. RESULTS

1st phase photon fluencies for 33 GHz Ka-Band, and 100 MHz modulation frequencies for 9th source-detector (SD) match at *x*, *y* top view can be seen in Figure 2, and Figure 3, respectively.

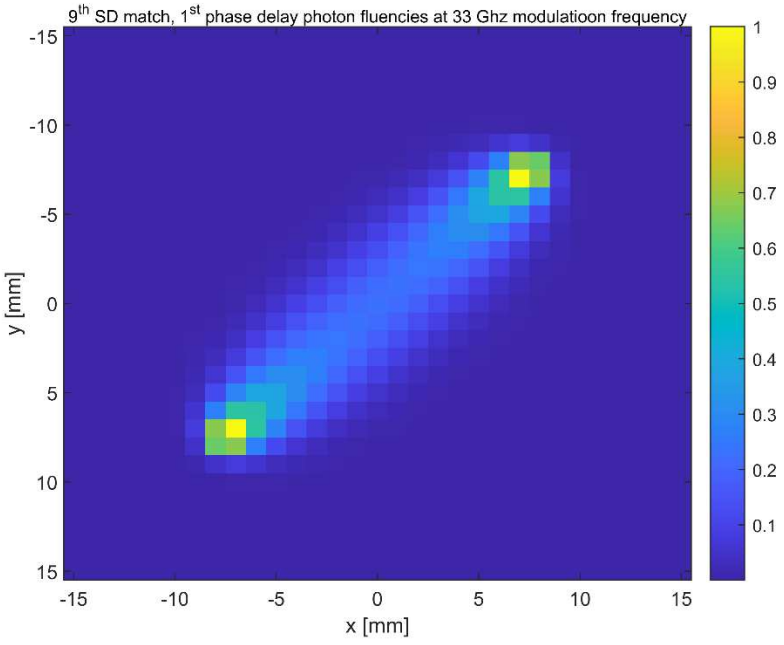

Figure 2. 9th source-detector (SD) match 1st phase photon fluencies at 33 GHz Ka-Band modulation frequency (top).

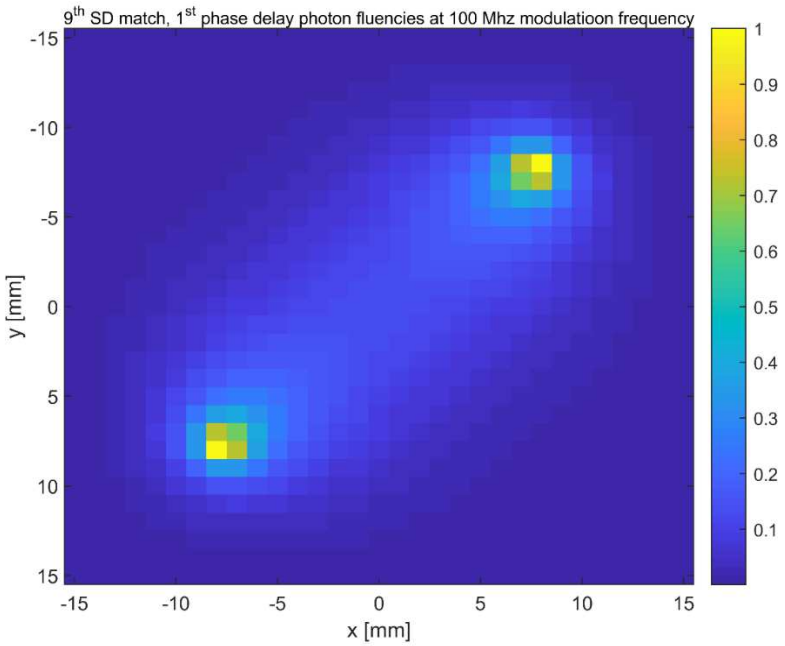

Figure 3. 9th source-detector (SD) match 1st phase photon fluencies at 100 MHz modulation frequency (top view).

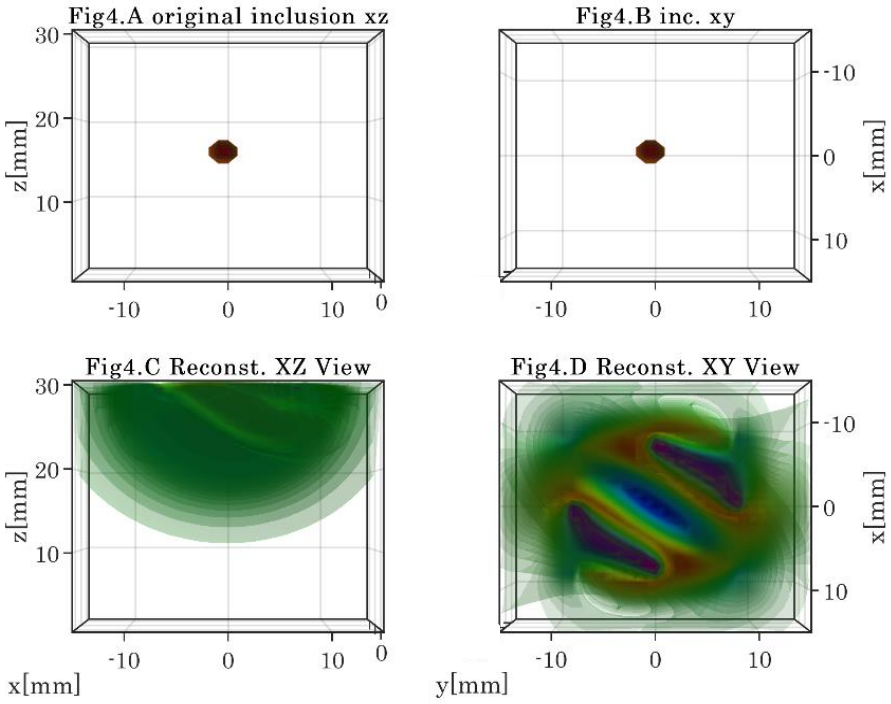

Figure 4. Original inclusion in Fig4.A (x, z view) and Fig4.B (x, y view), and reconstructed inclusion in Fig4.C (x, z view) and Fig4.D x, y view for 100 MHz modulation frequency.

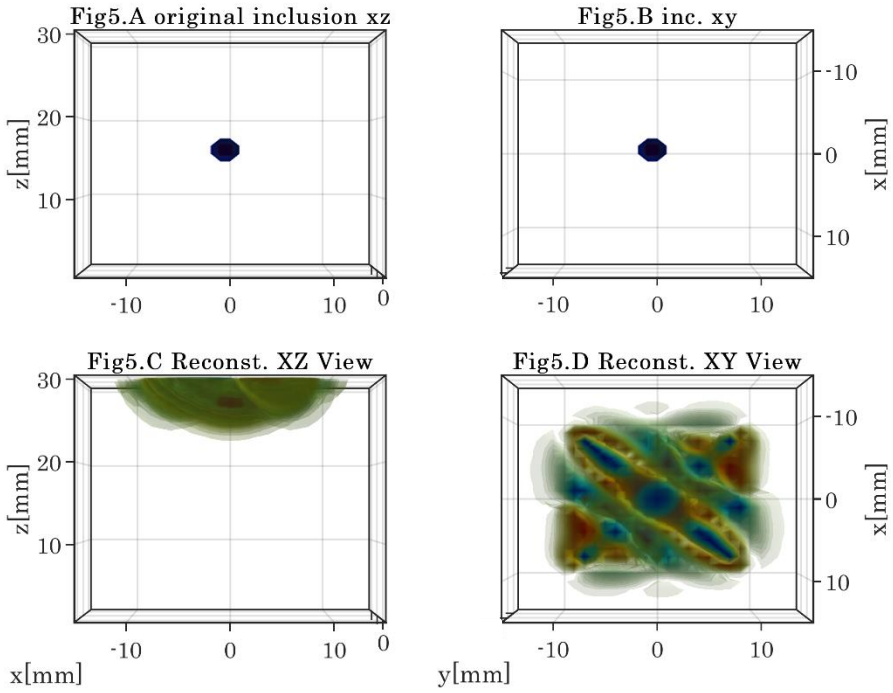

Figure 5. Original inclusion in Fig5.A (x, z view) and Fig5.B (x, y view), and reconstructed inclusion in Fig5.C (x, z view) and Fig5.D x, y view for 33 GHz Ka-Band modulation frequency.

Photon fluence distributions are different for both modulation frequencies. It would be assessed that forward model problem photon fluencies will affect the inverse problem solution algorithm of the imaging system; hence the reconstructed inclusion images will differ for each case. Basic pseudoinverse problem solution formula was applied to calculate the voxels' optic absorption coefficient μ_a at each modulation frequency. Original and reconstructed inclusions were illustrated for 100 MHz modulation frequency simulation case in Figure 4, and for 33 GHz Ka-Band modulation frequency simulation case in Figure 5. The photons for 100 MHz modulation frequency case are more scattered than the photons for 33 GHz Ka-Band modulation frequency simulation case. This situation eventually shows itself as more blurred reconstructed image for 100 MHz modulation frequency simulation case. If we compare the reconstructed inclusions of both simulation cases which are correspondent to the Figure 4.C, Figure 4.D, and Figure 5.C. and Figure

5.D, it would be realized that reconstructed inclusion for 33 GHz modulation frequency simulation case is more distinguishable than reconstructed inclusion for 100 MHz modulation frequency simulation case. Reconstructed inclusion can be recognized with the false depth resolution in 33 GHz simulation case, whereas there is no reconstructed inclusion in 100 MHz simulation case. From this comparison, it should be accepted that 33 GHz EHF band modulation frequency simulation case is superior to the 100 MHz simulation case.

IV. DISCUSSION

In this work, FDDOT BOI modality with two different modulation frequencies for back reflected DOT imaging geometry was tested and compared. Two different modulation frequencies 100 MHz, and 33 GHz Ka-Band were selected and compared with each other. 30 equal and sequential phase delays were added to both modulation frequencies and photon fluence distributions were calculated according to the diffusion equation (DE) in the frequency domain. One original inclusion was embedded inside the imaging geometry. The basic pseudoinverse problem solution algorithm was applied for both simulation cases. It was observed that, 33 GHz Ka-Band modulation frequency FDDOT simulation case is more trustable than the 100 MHz FDDOT simulation case, since the reconstructed inclusion image is sharper, and concentration is much cleaner. Signal to noise ratio (SNR) depends on the device capability. On the other hand, it was seen from this work that phase to noise ratio is getting better and reconstructed image quality is becoming sharper if the frequency increases. Hence, 33 GHz Ka-Band modulation frequency has better image reconstruction result.

V. CONCLUSION

Frequency comparison of FDDOT imaging methodology was presented in this paper. FDDOT imaging devices' light sources have been usually implemented by using 100 MHz modulation frequency in literature and research institutes. But in this work, it was shown that better results might have been taken by using extremely high frequency (EHF) band. Since the EHF band RF transmitter and receiver circuits have become more popular in biomedical imaging scientific community, electronic circuits would be implemented for this purpose. Despite the generally known and used literature knowledge of 100 MHz modulation frequency for FDDOT system modality, new Ka EHF-band frequency modulation was selected and used for FDDOT imaging system modality. It was observed that 33 GHz Ka-Band frequency modulation is more successful than generally accepted and tested 100 MHz frequency modulation laser tomography technique. Following this work, it is aimed to design and implement Ka EHF-band standard CMOS RF analog integrated circuit (IC) to implement the instrument and test for higher frequencies for FDDOT imaging systems. The FDDOT modality has been well developed and constructed for over 2 decades. The demonstrated simulation work shows the effect of using EHF band modulation frequency. It was illustrated that, by using 33 GHz modulation frequency, embedded inclusion was reconstructed not spatially as in right position but gave a better performance than 100 MHz modulation frequency which has been used by the academic society until now. There exists ultra-high speed long-reach and mode-locked laser diodes which can work in the Ka-Band modulation frequency range. For photodetector side, there exist 45-60 GHz Indium Galium Arsenic (InGaAs) photodetectors which can be used for future purposes.

Declaration of Interest: None

The author declares that he has no competing interests.

Financial competing interests:

• In the past five years the author has not received reimbursements, fees, funding, or salary from any organization that may in any way gain or lose financially from the publication of this manuscript, either now or in the future. The author works as Associate Prof. Dr. at a university that is not financing this manuscript (including the article-processing charge). The author has not held any stocks or shares in an organization that may in any way gain or lose financially from the publication of this manuscript, either now or in the future.

Funding: None

• The author does not hold, or he is not currently applying for any patents relating to the content of the manuscript. The author has not received reimbursements, fees, funding, or salary from an organization that holds or has applied for patents relating to the content of the manuscript.

• He does not have any other financial competing interests.

Non-Financial competing interests:

• There are no non-financial competing interests (political, personal, religious, ideological, academic, intellectual, commercial or any other) to declare in relation to this manuscript.

Ethical Approval: Not required

REFERENCES

1. Y. Hoshi, Y. Yamada, “Overview of diffuse optical tomography and its clinical applications,” J. of Biomed. Opt., **21**, 2016.

2. T. D. O’Sullivan, “Diffuse optical imaging using spatially and temporally modulated light,” J. of Biomed. Opt. **17**, 071311, 2012.

3. D. A. Boas, A. M. Dale, and M. A. Franceschini, “Diffuse optical imaging of brain activation: Approaches to optimizing image sensitivity, resolution, and accuracy,” NeuroImage **23**, S275–S288, 2004.

4. M. A. Franceschini et al., “Near-infrared spiroximetry: Noninvasive measurements of venous saturation in piglets and human subjects,” J. Appl. Physiol. **92(1)**, 372–384, 2002.

5. M. A. Franceschini and D. A. Boas, “Noninvasive measurement of neuronal activity with near-infrared optical imaging,” NeuroImage **21(1)**, 372–386, 2004.

6. B. Pogue B, M. Testorf, T. McBride, U. Osterberg, K. Paulsen, “Instrumentation and design of a frequency-domain diffuse optical tomography imager for breast cancer detection,” Opt. Exp., **1**, pp.391-403, Dec. 1997.

7. A. G. Orlova, I. V. Turchin, V. I. Plehanov, N. M. Shakhova, I. I. Fiks, M. I. Kleshnin, N. Y. Konuchenko, and V. A. Kamensky, “Frequency-domain diffuse optical tomography with single source-detector pair for breast cancer detection,” Laser Phys. Let., 5(4), 321, 2008.

8. M. Doulgerakis, A. T. Eggebrecht, H. Dehghani, “High-density functional diffuse optical tomography based on frequency-domain measurements improves image quality and spatial resolution,” Neurophotonics, **6**, 2019.

9. C. K. Hayakawa, K. Karrobi, V. Pera, D. Roblyer, and V. Venugopalan, “Optical sampling depth in the spatial frequency domain,” J. Biomed. Opt. 24(07), 1 (2018).

10. B. J. Tromberg, L. O. Svaasand, T.-T. Tsay, R. C. Haskell, and M. W. Berns, “Optical property measurements in turbid media using frequency-domain photon migration,” Proc. SPIE **1525**, 52–58, 1991.

11. F. Bevilacqua, A. J. Berger, A. E. Cerussi, D. Jakubowski, and B. J. Tromberg, “Broadband absorption spectroscopy in turbid media by combined frequency-domain and steady-state methods,” Appl. Opt. **39**(34), 6498–6507, 2000.

12. T. H. Pham, O. Coquoz, J. B. Fishkin, E. Anderson, and B. J. Tromberg, “Broad bandwidth frequency domain instrument for quantitative tissue optical spectroscopy,” Rev. Sci.

Instrum. **71**(6), 2500–2513, 2000.

13. T. O. McBride, B. W. Pogue, S. Jiang, U. L. Österberg, and K. D. Paulsen, "A parallel-detection frequency-domain near-infrared tomography system for hemoglobin imaging of the breast *in vivo*," Rev. Sci. Instrum. **72**(3), 1817–1824, 2001.

14. Y. Yang, H. Liu, X. Li, and B. Chance, "Low-cost frequency-domain photon migration instrument for tissue spectroscopy, oximetry, and imaging," Opt. Eng. **36**(5), 1562, 1997.

15. B. B. Zimmermann, Q. Fang, D. A. Boas, and S. A. Carp, "Frequency domain near-infrared multiwavelength imager design using high-speed, direct analog-to-digital conversion," J. Biomed. Opt. **21**(1), 016010, 2016.

16. L. Wang, and H. Wu, "*Biomedical Optics: Principles and Imaging*", John Wiley & Sons, Inc. New Jersey, 2007.

17. H. K. Kim, U. J. Netz, J. Beuthan, A. H. Hielscher, "Optimal source-modulation frequencies for transport-theory-based optical tomography of small-tissue volumes," Opt. Exp., **16**, 2008.

FIGURES DESCRIPTION

Figure 1. Four light sources (red circles) and detectors (blue squares) top view placement.

Figure 2. 9th source-detector (SD) match 1st phase photon fluencies at 33 GHz modulation frequency (top view).

Figure 3. 9th source-detector (SD) match 1st phase photon fluencies at 100 MHz modulation frequency (top view).

Figure 4. Original inclusion in Fig4.A (x, z view) and Fig4.B (x, y view), and reconstructed inclusion in Fig4.C (x, z view) and Fig4.D x, y view for 100 MHz modulation frequency.

Figure 5. Original inclusion in Fig5.A (x, z view) and Fig5.B (x, y view), and reconstructed inclusion in Fig5.C (x, z view) and Fig5.D x, y view for 41.8 GHz modulation frequency.

FIGURES

Figure 1

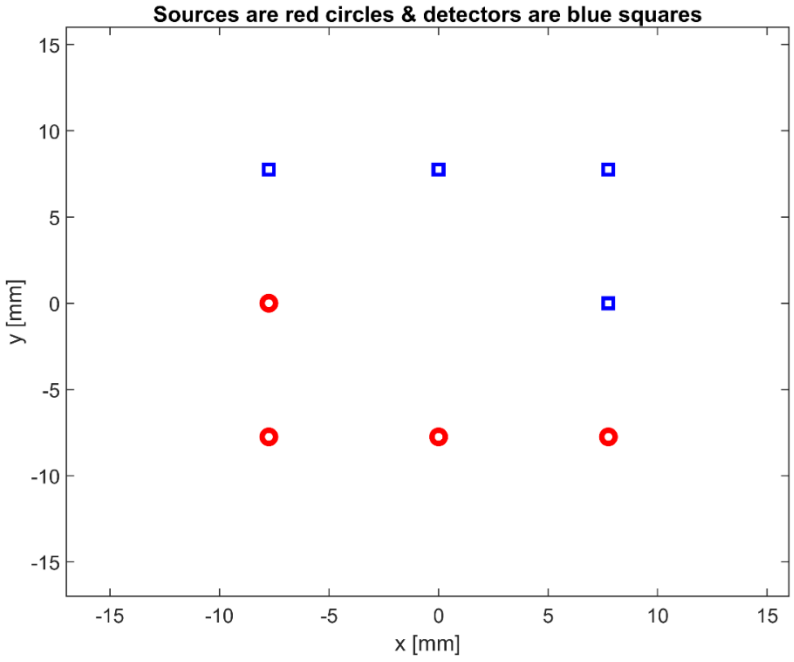

Figure 2

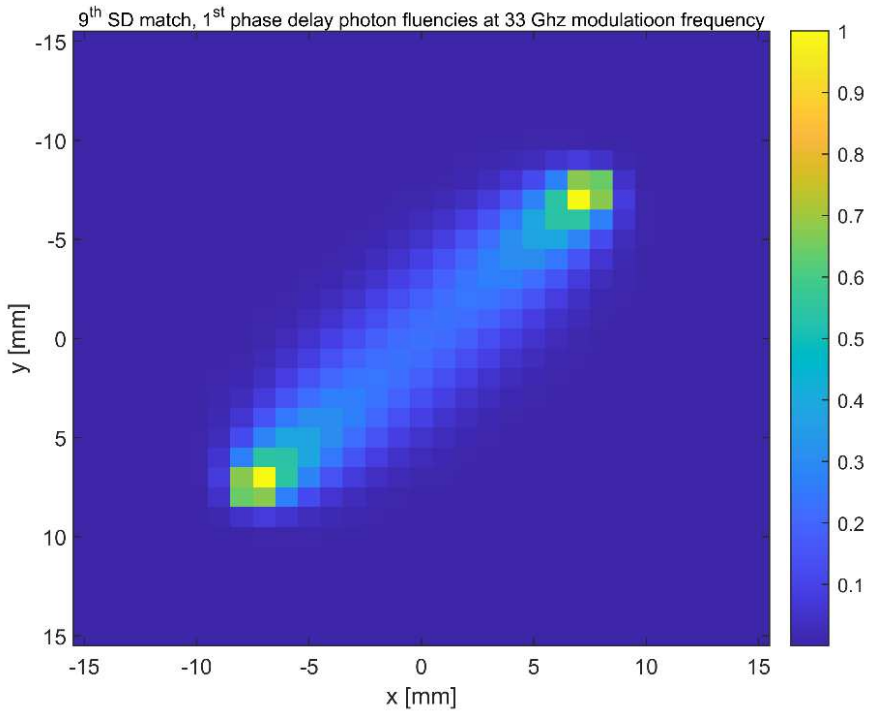

Figure 3

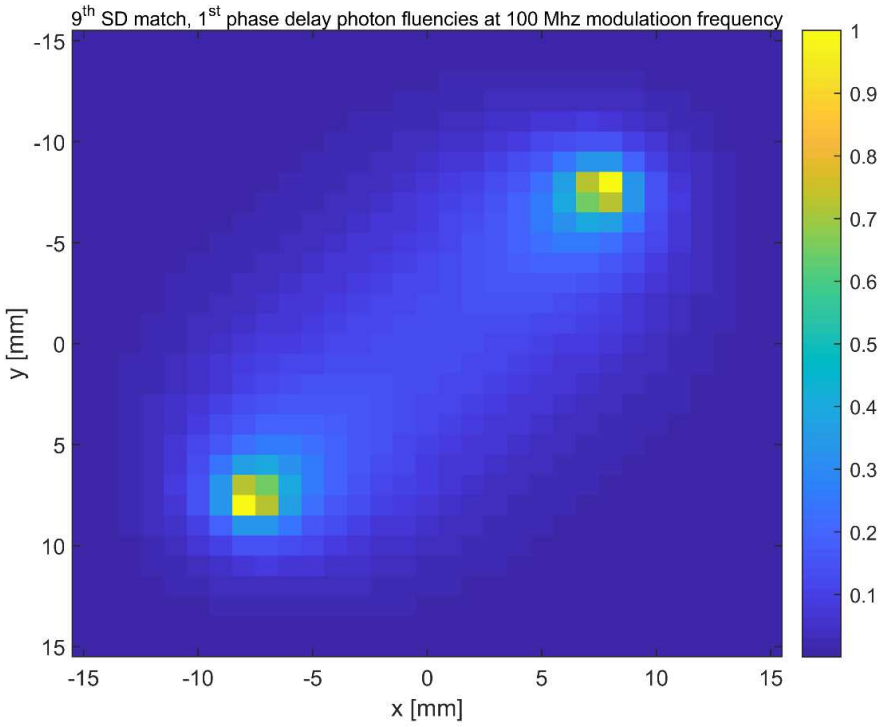

Figure 4

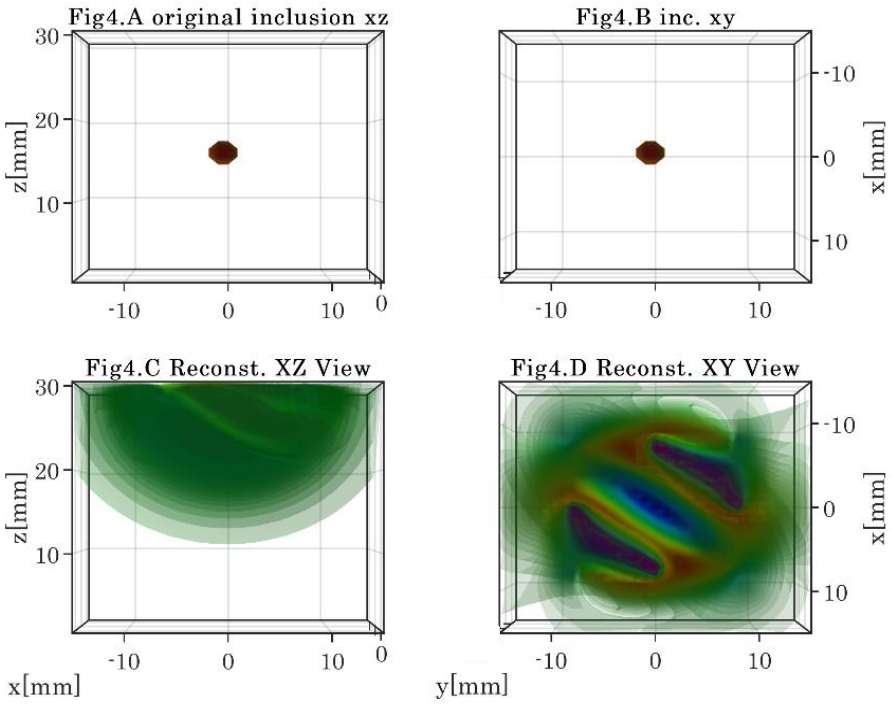

Figure 5

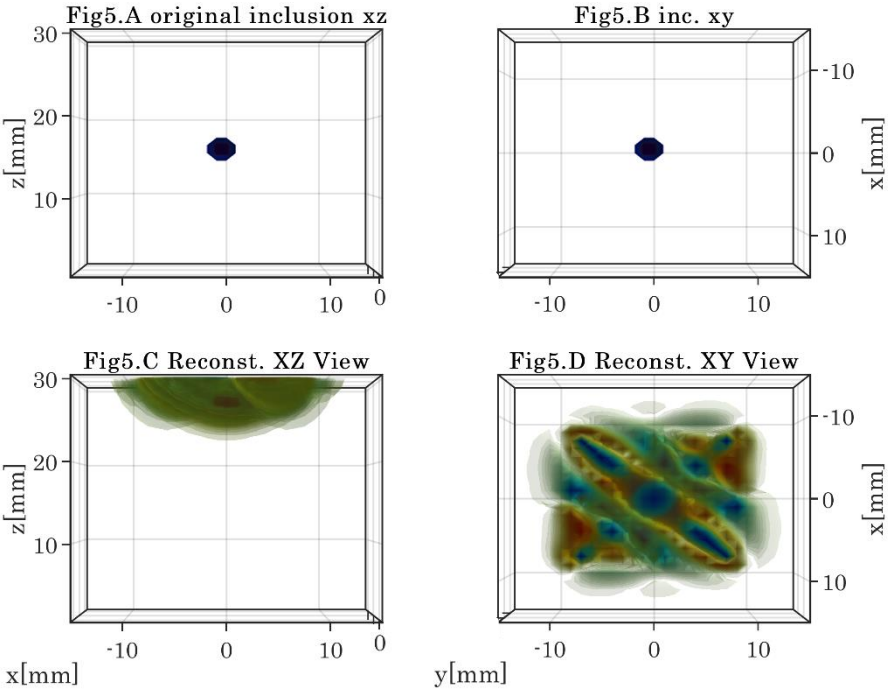

Figures

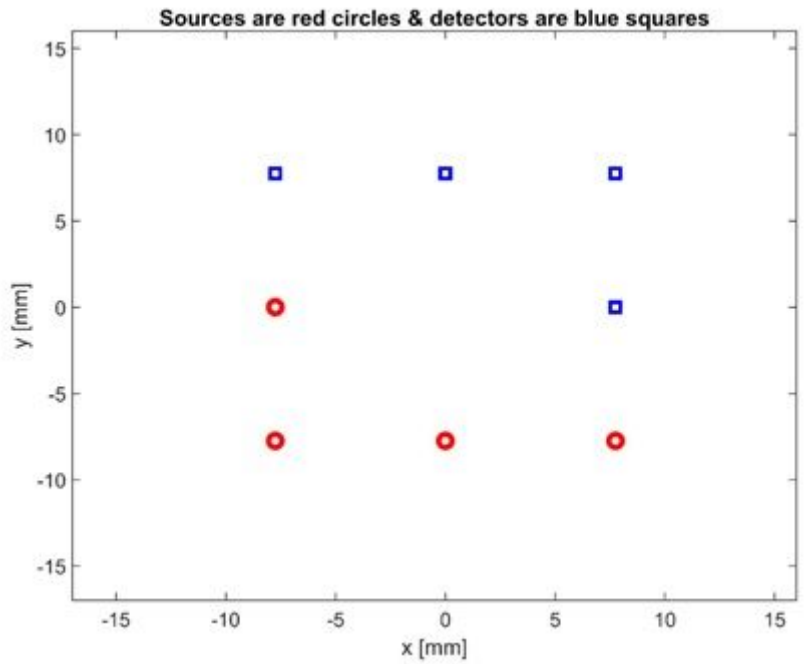

Figure 1

Four light sources (red circles) and detectors (blue squares) top view placement.

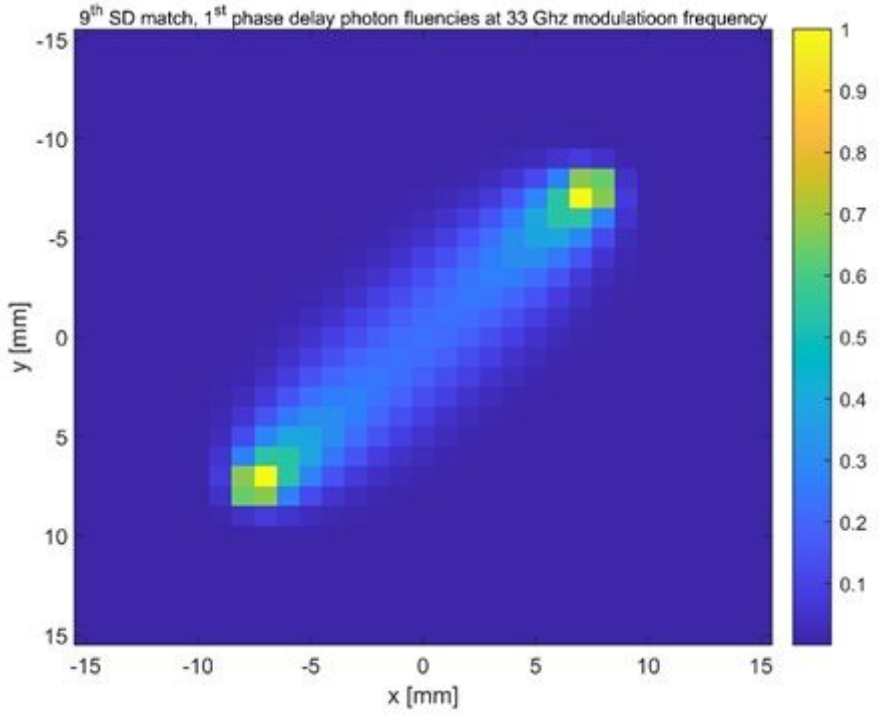

Figure 2

9th source-detector (SD) match 1st phase photon fluencies at 33 GHz modulation frequency (top view).

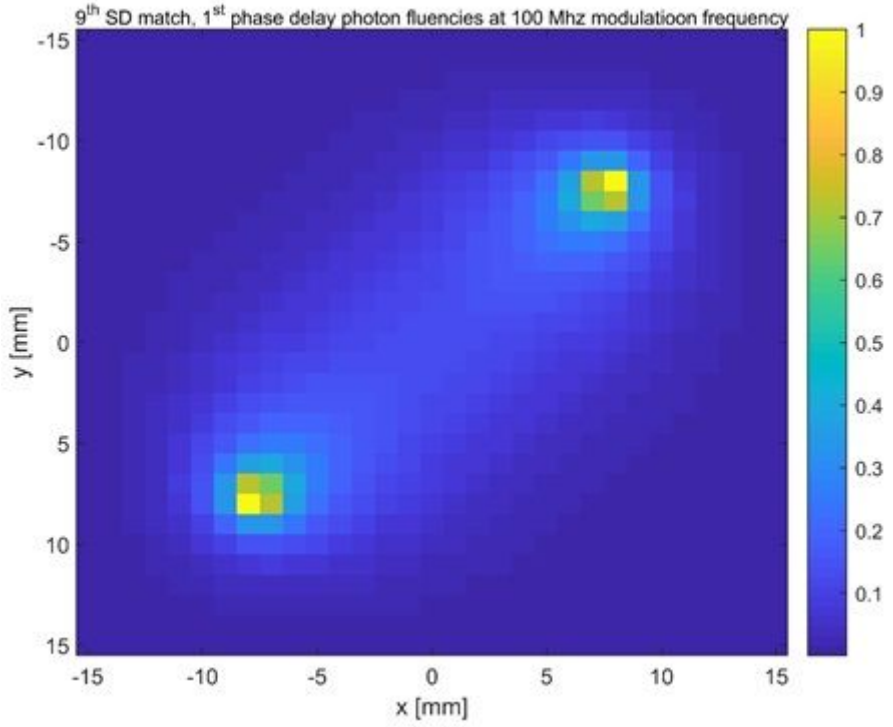

Figure 3

9th source-detector (SD) match 1st phase photon fluencies at 100 MHz modulation frequency (top view).

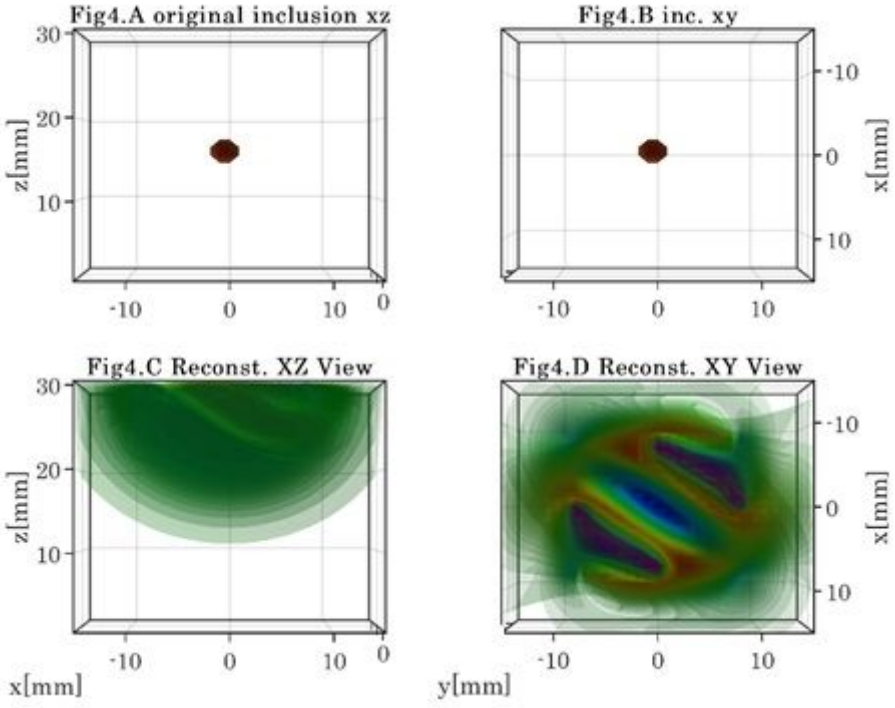

Figure 4

Original inclusion in Fig4.A (x, z view) and Fig4.B (x, y view), and reconstructed inclusion in Fig4.C (x, z view) and Fig4.D x, y view for 100 MHz modulation frequency.

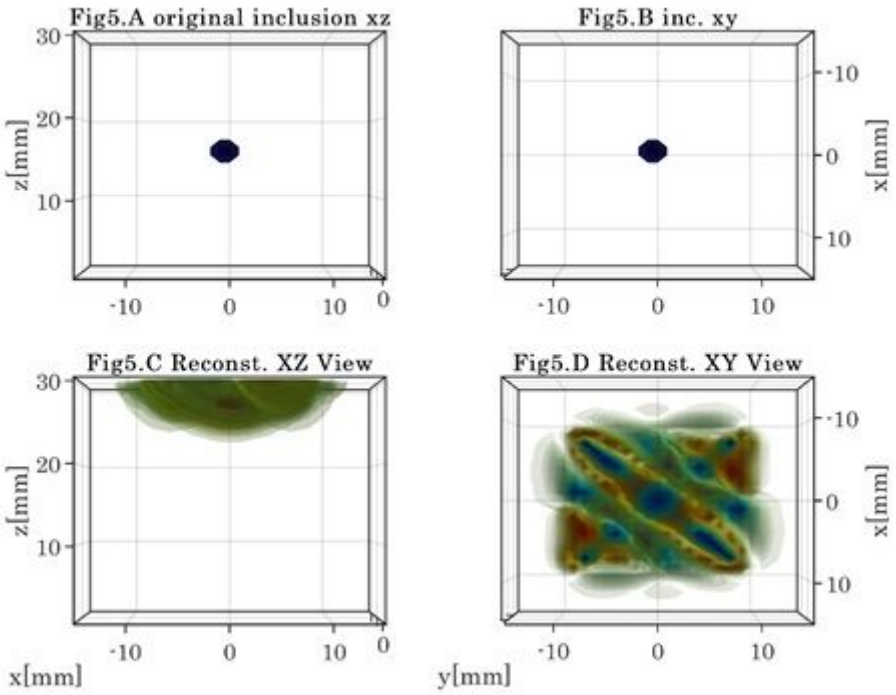

Figure 5

Original inclusion in Fig5.A (x, z view) and Fig5.B (x, y view), and reconstructed inclusion in Fig5.C (x, z view) and Fig5.D x, y view for 41.8 GHz modulation frequency.